



## Synchrotron-based FTIR evaluation of biochemical changes in cancer and noncancer cells induced by brominated marine coelenteramine

Carla M. Magalhaes<sup>a</sup>, Tanja Dučić<sup>b,\*\*</sup>, Renato B. Pereira<sup>c</sup>, Patricia González-Berdullas<sup>a</sup>, José E. Rodríguez-Borges<sup>d</sup>, David M. Pereira<sup>c</sup>, Joaquim C.G. Esteves da Silva<sup>a</sup>, Manuel Algarra<sup>e,\*\*\*</sup>, Luís Pinto da Silva<sup>a,\*</sup>

<sup>a</sup> Chemistry Research Unit (CIQUP), Institute of Molecular Sciences (IMS), Department of Geosciences, Environment and Territorial Planning, Faculty of Sciences, University of Porto, Rua do Campo Alegre s/n, 4169-007, Porto, Portugal

<sup>b</sup> ALBA CELLS Synchrotron, Carrer de la Llum 2-26 08290 Cerdanyola del Vallès, Barcelona, Spain

<sup>c</sup> REQUIMTE/LAQV, Laboratório de Farmacognosia, Departamento de Química, Faculdade de Farmácia, Universidade do Porto, Rua de Jorge Viterbo Ferreira, N° 228, 4050-213, Porto, Portugal

<sup>d</sup> LAQV/REQUIMTE, Department of Chemistry and Biochemistry, Faculty of Sciences, University of Porto, Rua do Campo Alegre s/n, 4169-007, Porto, Portugal

<sup>e</sup> INAMAT2 - Institute for Advanced Materials and Mathematics, Department of Science, Public University of Navarra, Campus de Arrosadía, 31006, Pamplona, Spain

### ARTICLE INFO

#### Keywords:

FTIR  
Synchrotron radiation  
Anticancer therapy  
Coelenteramine  
Coelenterazine  
Bioluminescence

### ABSTRACT

The mode of action toward gastric cancer cells of brominated Coelenteramine, an analogue of a metabolic product of a marine bioluminescent reaction, was investigated by synchrotron radiation-based Fourier Transform Infrared spectroscopy (FTIR). This method revealed that the anticancer activity of brominated Coelenteramine is closely connected with cellular lipids, by affecting their organization and composition. More specifically, there is an increasing extent of oxidative stress, which results in changes in membrane polarity, lipid chain packing and lipid composition. However, this effect was not observed in a noncancer cell line, helping to explain its selectivity profile. Thus, synchrotron radiation-based FTIR helped to identify the potential of this Coelenteramine analogue in targeting membrane lipids, while proving to be a powerful technique to probe the mechanism of anticancer drugs.

### 1. Introduction

Despite improvements in therapy, cancer is still one of the major health problems worldwide [1]. Indeed, many patients still cannot escape therapy failure and serious side effects [2]. Developing new anticancer drugs is also complex and with high rates of failure at the clinical trial stage due to problems with efficacy or toxicity [3]. One of the reasons for that is that different compounds can act via off-target effects [3]. For this reason, more detailed investigations of the mode of action of potential drugs are needed at preclinical stages [3]. A better understanding of the mechanism of action of novel molecules with anticancer properties can also help to identify new targets for cancer therapy [4].

Bioluminescence (BL) is a remarkable phenomenon in which light emission occurs due to a biochemical reaction [5,6], which has been

gaining applications in biomedical and bioanalytical fields [7,8]. Among the most well-known BL systems is that of Coelenterazine (Clz, Scheme 1), a molecule widely found in marine organisms [5]. One of the components of this system is Coelenteramine (Clm, Scheme 1), which is a metabolic product of Clz-based BL reactions [9–11]. Recently, we have found out that a brominated Clm analogue (Br-Clm, Scheme 1) had anticancer activity toward gastric (AGS) cancer cells, with IC<sub>50</sub> values ranging from 54.3 μM to 15.2 μM (depending on the incubation period) [9]. This compound also showed cytotoxicity (albeit more reduced) towards a lung cancer cell line [9]. Interestingly, Br-Clm only showed residual toxicity (~10% at 100 μM) towards noncancer keratinocytes (HaCaT cells), thereby showing an interesting selectivity profile toward cancer cells [9]. Also, when used in combination, Br-Clm was able to enhance the activity of a chemotherapeutic agent [10]. Thus, this compound shows potential for further optimizations toward obtaining a

\* Corresponding author.

\*\* Corresponding author.

\*\*\* Corresponding author.

E-mail addresses: [tducic@cells.es](mailto:tducic@cells.es) (T. Dučić), [manuel.algarra@unavarra.es](mailto:manuel.algarra@unavarra.es) (M. Algarra), [luis.silva@fc.up.pt](mailto:luis.silva@fc.up.pt) (L. Pinto da Silva).

<https://doi.org/10.1016/j.abbi.2023.109660>

Received 31 March 2023; Received in revised form 19 May 2023; Accepted 30 May 2023

Available online 30 May 2023

0003-9861/© 2023 The Authors. Published by Elsevier Inc. This is an open access article under the CC BY license (<http://creativecommons.org/licenses/by/4.0/>).

safer and more effective anticancer agent.

Nevertheless, this pursuit is impaired by the lack of information regarding the mode of action of Br-Clm, which was shown to activate effector caspases while the upstream target responsible for this was not identified [9,10]. Thus, a comprehensive understanding of how Br-Clm affects both cancer and noncancer cells is needed. Relevant insights regarding this could be obtained by examining how Br-Clm affects the biomolecular composition and conformations in both cancer and noncancer cells by infrared spectroscopy.

Herein, synchrotron radiation-based FTIR (SR-FTIR) microspectroscopy was used to investigate the biochemical changes induced by Br-Clm on both gastric cancer (AGS) and noncancer keratinocytes (HaCaT) cell lines. SR-FTIR is a label-free and nondestructive approach that allows probing the biochemical composition of biological systems, including cells [12]. The application of synchrotron radiation as the source of infrared light can combine the highest spectral and spatial resolution to achieve single-cell resolution [12,13]. Thus, it can provide detailed information about the composition and conformational organization of different classes of biomolecules [12–14]. In this way, variations in specific spectral signatures after treatment with target compounds can be related to their mode of action [15,16].

## 2. Material and methods

### 2.1. Br-Clm

Br-Clm was already reported and was prepared by the procedure previously described by us [9–12]. Namely, by a Suzuki-Miyaura cross-coupling reaction between 5-bromopyrazin-2-amine and 4-bromophenylboronic acid [9–12].

### 2.2. Preparation of cell samples

AGS and HaCaT cell lines were purchased from ATCC (Manassas, VA, USA) and maintained in medium DMEM + GlutaMAX™ with 1% penicillin/streptomycin and 10% FBS, at 37 °C, in a humidified atmosphere of 5% CO<sub>2</sub>. Cells were seeded in 48-well plates at a density of 30,000 cells/well at 24 h and allowed to attach in glass coverslips (Crystan, UK, CaF<sub>2</sub> 10 mm × 0.5 mm) for 24 h under the conditions described above. Then, cells were incubated for a period of 24 h with Br-Clm at a concentration of 50 μM. Samples were prepared in triplicate. After the incubation period, the cells were washed with HBSS (Hanks' balanced salt solution) and fixed with 4% paraformaldehyde for 20 min at room temperature, washed with water and kept dry over silica gel.

The concentration at which both cell lines were incubated with Br-Clm (50 μM) is near the IC<sub>50</sub>, in this incubation time, of this compound for AGS cells (54.3 μM), while having no effect on the cellular viability of HaCaT cells [9]. So, it was deemed a good choice for understanding both the mode of action and selectivity profile of Br-Clm.

### 2.3. SR-FTIR spectroscopy

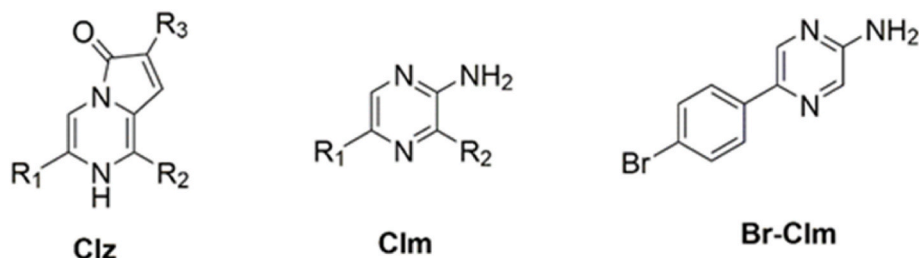
The SR-FTIR measurements were carried out at the MIRAS beamline

at the synchrotron ALBA (Barcelona, Spain) [17], by using procedures previously followed by us [13–15,18]. Namely, the synchrotron light was used as the infrared light source. The infrared (IR) spectra were collected in a transmission mode using a 3000 Hyperion microscope coupled to an FTIR Vertex 70v spectrometer and a liquid nitrogen-cooled mercury cadmium telluride (MCT) detector. The aperture slits were set to 10 × 10 μm to achieve the single-cell size, and 30 cells for each sample were analyzed. Each spectrum was acquired after 256 co-added scans per spectrum, at 4 cm<sup>-1</sup> spectral resolution. The spectroscopic data were collected in transmission mode using the 36 × Schwarzschild objective and condenser. Spectra for each treatment were collected in the 4000–700 cm<sup>-1</sup> mid-infrared range. The OPUS 8.2 (Bruker, Germany) software package was used for data acquisition. The SR-FTIR spectra were processed by using the Quasar Spectroscopy tools, which allow multimodal spectral analysis involving the principal component analysis (PCA) [19]. Rubber band baseline correction and vector normalization were performed for each single spectrum. For the second derivative calculations, the Savitzky-Golay filter was applied with smoothing points 13, and polynomial order 3 for spectral range as indicate in respective Figures.

## 3. Results and discussion

SR-FTIR was employed to evaluate the biochemical changes induced by incubating cancer AGS and noncancer HaCaT cell lines with Br-Clm, by following procedures used before by members of this team [13–15, 18]. To that end, two different regions of interest in the SR-FTIR spectra were analyzed, regarding the spectra obtained for treated and untreated (control) cells with Br-Clm. The first part of the spectra is at 3100–2800 cm<sup>-1</sup> (Fig. 1), which is crucial for lipid analysis [15]. Namely, it is associated with contributions from carbon-hydrogen stretching vibrations ( $\nu(\text{C-H})$ ) that originate from lipids' fatty acid chains [14,15]. The most intense bands for all cases were that at 2925 and 2955 cm<sup>-1</sup>, which correspond to the asymmetric vibration of methylene ( $\nu_{as}(\text{CH}_2)$ ) and methyl ( $\nu_{as}(\text{CH}_3)$ ) groups, respectively [14,15]. The bands corresponding to symmetric  $\nu_s(\text{CH}_2)$  and  $\nu_s(\text{CH}_3)$  are those found at 2850 and 2870 cm<sup>-1</sup> [14,15]. The less intense band at 3060 cm<sup>-1</sup> can be attributed to  $\nu(\text{C=C-H})$ .<sup>15</sup> Analysis of both sets of data (cancer/noncancer, Fig. 1A and B) revealed spectra that are qualitatively dissimilar, despite showing that both cell lines were affected.

For AGS cells (Fig. 1A), treatment with Br-Clm increased the intensity of bands associated with  $\nu_{as}(\text{CH}_3)$  and  $\nu_{as}(\text{CH}_2)$ , while reducing the intensity of  $\nu_s(\text{CH}_2)$ ,  $\nu_s(\text{CH}_3)$  and  $\nu(\text{C=C-H})$ . It should be noted that a decrease in the  $\nu(\text{C=C-H})$  band is possibly caused by lipid peroxidation [15]. Consistently, an increase of the  $\nu_{as}(\text{CH}_2)$  band (observed in AGS cells upon treatment with Br-Clm) can also indicate an increased level of oxidative stress [18]. Furthermore, treatment of AGS cells with Br-Clm also led to a shift of the  $\nu_{as}(\text{CH}_3)$ ,  $\nu_s(\text{CH}_3)$  and  $\nu_{as}(\text{CH}_2)$  bands to higher wavenumbers, which can indicate changes in membrane fluidity caused by oxidative modification of lipids [15,18]. Quite interestingly, these specific variations of spectral data were not found for HaCaT cells upon treatment with Br-Clm (Fig. 1B), despite this compound also exerting some effect on cellular lipids. A more quantitative evaluation of



**Scheme 1.** Schematic representation of Clz, Clm and Br-Clm. R<sub>1</sub>: phenol. R<sub>2</sub>: benzyl. R<sub>3</sub>: *p*-cresol.

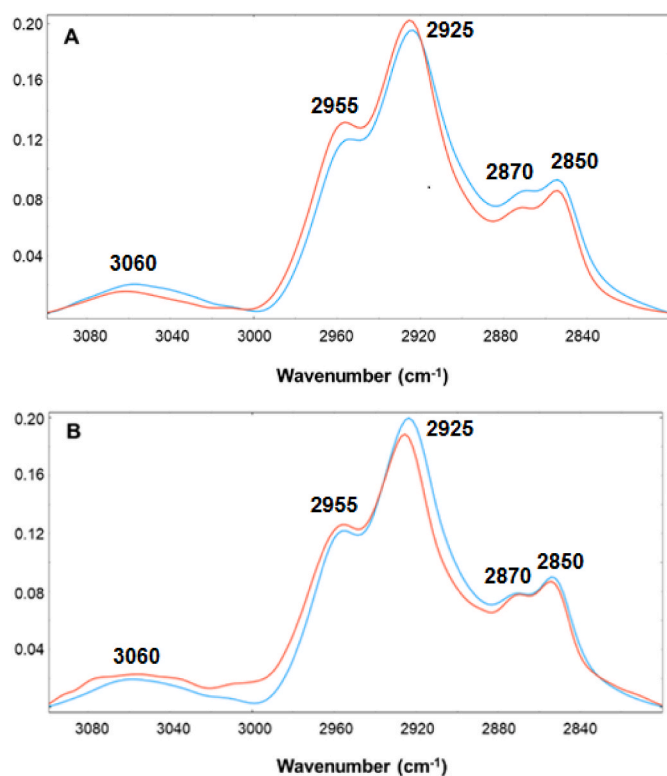


**Fig. 1.** Average SR-FTIR spectra, in the area of 3100–2800  $\text{cm}^{-1}$ , of AGS (A) and HaCaT (B) cells, when treated (red) or untreated (blue) with Br-Clm (50  $\mu\text{M}$ ).

the effect exerted by Br-Clm was performed by calculating the  $\nu_{\text{as}}(\text{CH}_2)/\nu_{\text{as}}(\text{CH}_3)$ ,  $\nu_{\text{as}}(\text{CH}_2)/\nu_{\text{s}}(\text{CH}_3)$  and  $\nu_{\text{s}}(\text{CH}_2)/\nu_{\text{s}}(\text{CH}_3)$  ratios. These ratios are related to the degree of saturation [15], membrane polarity [21], and lipid chain packing [15,20], respectively.

Br-Clm decreased the value of  $\nu_{\text{as}}(\text{CH}_2)/\nu_{\text{as}}(\text{CH}_3)$  ratio in both AGS ( $2.83 \pm 0.08$  to  $2.26 \pm 0.04$ ) and HaCaT ( $2.73 \pm 0.05$  to  $2.12 \pm 0.08$ ) cell lines, indicating that fatty acid chains become shorter upon addition of the studied compound (irrespective of the studied cell line) [15].

Noticeably, the calculation of other ratios revealed significant differences regarding the interaction of Br-Clm with cancer and non-cancer cells. Upon treatment with Br-Clm, the value of  $\nu_{\text{as}}(\text{CH}_2)/\nu_{\text{s}}(\text{CH}_3)$  increased in AGS cells ( $5.41 \pm 0.07$  to  $6.11 \pm 0.04$ ) while remaining essentially the same in HaCaT cells ( $5.80 \pm 0.08$  to  $5.61 \pm 0.17$ ). Therefore, Br-Clm appears to increase the polarity of the membrane in cancer cells [21], while having no effect on the polarity of the membrane of non-cancer cells. A similar case was seen for  $\nu_{\text{s}}(\text{CH}_2)/\nu_{\text{s}}(\text{CH}_3)$  ratio, which decreased in AGS ( $1.57 \pm 0.02$  to  $1.49 \pm 0.02$ ), while remaining the same in HaCaT cells ( $1.61 \pm 0.02$  to  $1.64 \pm 0.04$ ). Meaning that Br-Clm reduces lipid chain packing in cancer cells, while having no effect in the same parameter in noncancer cells. So, it is clear that Br-Clm has a relevant effect on cellular lipids in cancer cells apparently related to oxidative stress, which might help to explain its anticancer mode of action [9]. Also, these effects are less obvious or even absent in non-cancer cells [9,10].

The second region of interest is in the interval of 1800–900  $\text{cm}^{-1}$  (Fig. 2), in which can be found bands characteristics of lipids, proteins, nucleic acids, and carbohydrates [14–16,18,20]. More specifically, the sub-interval of 1800–1480  $\text{cm}^{-1}$  mainly contains absorption bands associated with protein Amide I (at 1640  $\text{cm}^{-1}$ ) and Amide II (at 1535  $\text{cm}^{-1}$ ) [16,18] which are quite sensitive to the secondary structure of proteins [14,20]. A band at 1740  $\text{cm}^{-1}$  can also be found here, which is associated with the stretching vibration of carbonyl groups ( $\nu(\text{C}=\text{O})$ ) of lipid esters [15].

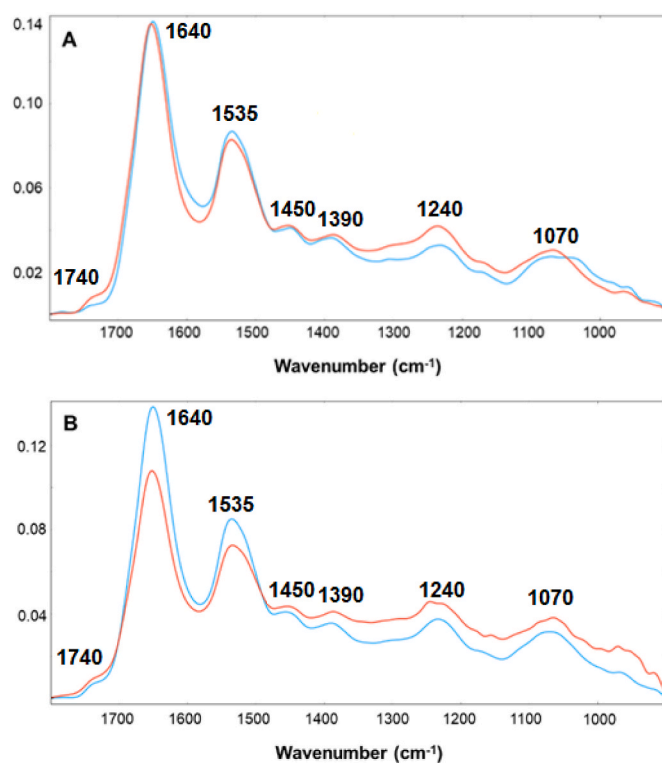


**Fig. 2.** Average SR-FTIR spectra, in the area of 1800–900  $\text{cm}^{-1}$ , of AGS (A) and HaCaT (B) cells, when treated (red) or untreated (blue) with Br-Clm (50  $\mu\text{M}$ ).

The treatment with Br-Clm of AGS cells (Fig. 2A) only led to small differences regarding Amide I and II, as the intensity is only slightly decreased (more evident in Amide II) and only slight shifts to higher wavenumbers were observed. This is not the case, however, for the treatment of HaCaT cells (Fig. 2B). In this case, there are relevant decreases in intensity for both Amide I and II. Thus, treatment with Br-Clm leads to changes in protein structures for both cell lines, but with higher impact in noncancer HaCaT cells. However, it should be noted that at the concentration used for Br-Clm, this compound only led to cytotoxicity toward cancer cells and not noncancer ones [9]. So, these changes are most likely not related to the anticancer mechanism of this compound. Nevertheless, the effect of Br-Clm on the protein conformational changes was evaluated by examining the second derivative of the Amide I part of the spectra (Fig. 3), which is associated with changes in protein secondary structures [16,18,20]. The most prominent bands in all of those spectra were at  $\sim 1685$  and  $\sim 1655$   $\text{cm}^{-1}$ , and a shoulder at  $\sim 1635$   $\text{cm}^{-1}$ . These correspond to turn and loops,  $\alpha$ -helix, and  $\beta$ -sheet structure, respectively [14]. While quantitative differences are visible in the effect exerted by treatment with Br-Clm on both AGS and HaCaT cells, we can observe some qualitative similarities between both datasets. That is, while treatment with Br-Clm leads to changes in all bands/shoulders, these differences are lower at  $\sim 1685$ , and more significant at  $\sim 1655$  and  $\sim 1635$ . Thus, Br-Clm influences the secondary structure of proteins, particularly the  $\alpha$ -helix and  $\beta$ -sheet structure.

Regarding the carbonyl  $\nu(\text{C}=\text{O})$  group (Fig. 2), the band intensity is increased upon treatment with Br-Clm for both cell lines. It should be noted that this band could result from the peroxidation of fatty acid chains. Therefore, an increase in this peak area is an indicator of an increase in lipid peroxidation [15]. This band increased in both AGS (from  $0.15 \pm 0.02$  to  $0.30 \pm 0.01$ ) and HaCaT cells (from  $0.22 \pm 0.01$  to  $0.32 \pm 0.02$ ). These values indicate that lipid peroxidation is induced by Br-Clm in both cell lines. However, it is higher in the AGS cell line, and it confirms that this compound has a more pronounced effect on cancer cell lipids.

Finally, the sub-interval of 1480–900  $\text{cm}^{-1}$  (fingerprint region)

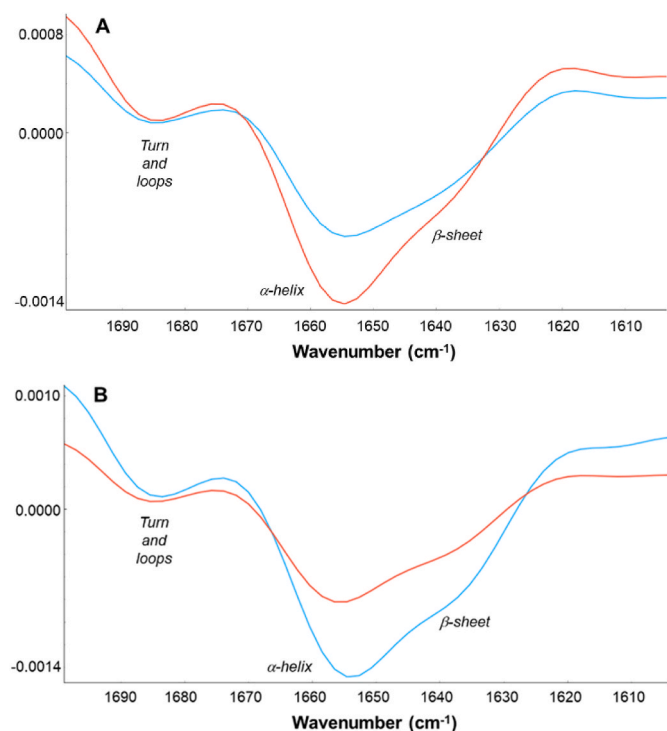


**Fig. 3.** Second-derivative of the average SR-FTIR spectra, in the area of 1700–1600  $\text{cm}^{-1}$ , of AGS (A) and HaCaT (B) cells, when treated (red) or untreated (blue) with Br-Clm (50  $\mu\text{M}$ ).

contains several bands that are typically associated with lipids, proteins, nucleic acids, and carbohydrates. Namely, two bands at 1450 and 1390  $\text{cm}^{-1}$ , which are attributed to bending vibrations of unsaturated aliphatic chains, and vibrations of carboxylic acids and/or aldehydes are observed (Fig. 2) [18]. These two bands can be associated with both lipids and proteins [16,18]. Interestingly, in AGS cells the treatment with Br-Clm did not lead to relevant changes in these bands, contrary to what happened in HaCaT cells. Regarding the different effects exerted by Br-Clm on cancer and noncancer cells, it is possible to assume that these bands could have higher contributions from proteins.

Shoulders between 1200 and 1150  $\text{cm}^{-1}$  are seen in all datasets (Fig. 2), which are expected to be related to  $\nu(\text{C}-\text{C})$ ,  $\nu(\text{C}-\text{O}-\text{C})$  and  $\nu(\text{C}-\text{OH})$  vibrations of carbohydrates [16]. Nevertheless, these appear to not be particularly changed.

Other bands of potential interest are found at 1240 and 1070  $\text{cm}^{-1}$ , which are typically associated with phosphate asymmetric ( $\nu_{\text{as}}(\text{PO}_4^{2-})$ ) and symmetric ( $\nu_{\text{s}}(\text{PO}_4^{2-})$ ) stretch vibrations of DNA and RNA backbones (i.e. nucleic acids) [16,18]. We can see that treatment with Br-Clm resulted in an increase of these bands for both cell lines (Fig. 2). This increase appears to be similar in both cell lines for  $\nu_{\text{as}}(\text{PO}_4^{2-})$ . However, the difference in intensities for  $\nu_{\text{s}}(\text{PO}_4^{2-})$  is lower in AGS than in HaCaT cells, which indicates that there is here a relevant distinction regarding the effect of Br-Clm. Below 1000  $\text{cm}^{-1}$ , absorption bands associated with nucleic acids can be found, as well as phosphorylated proteins [16]. More specifically, these bands are associated with the symmetric stretching of di-anionic phosphate monoesters [16]. These bands can be seen in the spectra for both cell lines (Fig. 2). However, while incubation with Br-Clm leads to relevant differences in HaCaT cells, this is not the case for AGS cells (Fig. 2). Therefore, incubation with Br-Clm does affect nucleic acids in these two cell lines. However, the observed effect appears to be more pronounced in HaCaT than in AGS cells. Thus, these changes are not expected to be related to the mechanism of anticancer cancer of Br-Clm [9]. Also, as this concentration of Br-Clm (50  $\mu\text{M}$ ) has no effect on the cellular viability of HaCaT [9], these changes do not appear to result directly in cytotoxicity.

In short, Br-Clm appears to induce biochemical changes in both cancer and noncancer cells, by having effects on biomolecules such as lipids, proteins, and nucleic acids. However, the effect on cellular lipids appears to be associated with the previously observed anticancer activity and selectivity profile of Br-Clm [9,10]. In fact, lipid metabolism is deregulated in cancer [22]. Moreover, lipids are the major components of cellular membranes and are responsible for regulating membrane functions. Finally, cellular membranes of cancer and noncancer cells possess relevant differences in lipid composition [22]. Thus, targeting membrane lipids has been explored as a promising anticancer therapy, with enhanced sensitivity to cancer cells [22]. The current study provided information that allows us to associate the mode of action of Br-Clm with the modulation of membrane lipid composition/organization [22].

Thus, we performed PCA multivariate statistical analysis to further explore the alterations in AGS cells' lipids induced by Br-Clm (Fig. 4) [16]. PCA analysis reflects not only spectral data but also relevant differences between samples [16]. The PCA analysis is presented after performing the second derivative of the SR-FTIR. The PCA score plot (Fig. 4) describes 93% of data variability, while PC1 and PC2 explained 86% and 7% of total variance. The score plot showed that the datasets are clustered into different groups, with Br-Clm-treated cells showing mostly positive PC1 scores (please note that it is opposite proportional after derivation), while the control ones presented mainly negative PC1 scores. The loading plot PC1 minimum value was observed at  $\sim 2924 \text{ cm}^{-1}$ , associated with the asymmetric vibration of  $\text{CH}_2$  groups, and  $\sim 2965 \text{ cm}^{-1}$ , related to the asymmetric vibration of  $\text{CH}_3$  groups, which is more pronounced in treated cells. Analysis of the PC1 loadings showed higher absolute values in wavenumbers associated with the vibrations of methyl and methylene groups, pointing out the shorter chains of lipids in

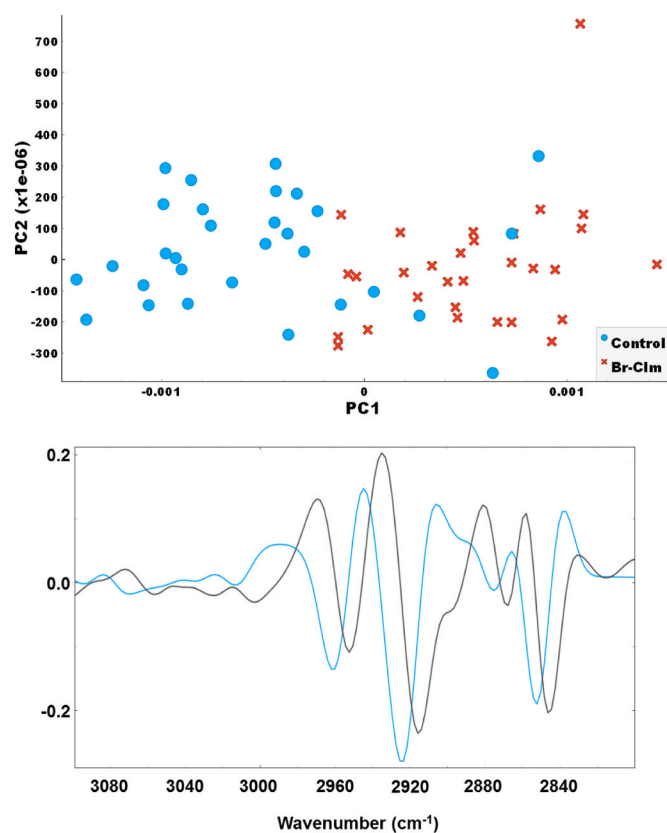


**Fig. 4.** PCA score plot for the area of 3100–2800  $\text{cm}^{-1}$ , regarding AGS cell lines treated and untreated with Br-Clm (top). Corresponding PCA loadings of the first two components, PC1 (blue) and PC2 (dark gray), regarding the interval of 3100–2800  $\text{cm}^{-1}$  (bottom).

treated cells, and the possible effect of lipids peroxidation.

Next, we have also performed PCA analysis to explore the alterations in AGS cells induced by Br-Clm, within the area of 1800–1480  $\text{cm}^{-1}$  (Fig. 5). The PCA score plot describes 90% of data variability, while PC1 and PC2 explained 81% and 9% of the total variance. Analysis of the score plot indicates that Br-Clm-treated cells are mainly clustered in positive PC1 scores, while control cells are primarily clustered in negative PC1 scores. The loadings plot showed the maxima at  $\sim 1655$  and  $1540 \text{ cm}^{-1}$ , associated with  $\alpha$ -helix, and minima at  $\sim 1620$  and  $\sim 1717 \text{ cm}^{-1}$ , connected to aromatic residues and carboxyl group. These subtle changes are associated with changes in protein secondary structures [16,18,20]. Thus, according to the loading plot, we can conclude that Br-Clm treatment influences positively on  $\alpha$ -helix structure, as well as the random coil, while control samples contained more tyrosine and phenylalanine residues in proteins and carboxyl groups.

Finally, given that the mode of action of Br-Clm appears to be related to alterations of cellular lipids, we have provided the second-derivative of the SR-FTIR spectra in the area of 3100–2800  $\text{cm}^{-1}$  for both AGS and HaCaT cells. These spectra are presented in Fig. 6. Regarding treated and control AGS cells, the main observed differences are related to wavenumbers associated with asymmetric and symmetric vibrations of methylene groups, and asymmetric vibrations of methyl groups, pointing out different ratios of  $\text{CH}_2$  vs  $\text{CH}_3$  groups observed in lipids peroxidation [23]. Interestingly, when we analyze treated and control HaCaT cells, we reach to the same qualitative conclusion. That is, the main difference between datasets appears to be related to the vibrations of long acyl chains in membrane lipids. However, the differences between treated and control groups are opposite when we compare AGS and HaCaT datasets. So, these results further indicate that the different effects exerted by Br-Clm on AGS and HaCaT are related to cellular lipids,

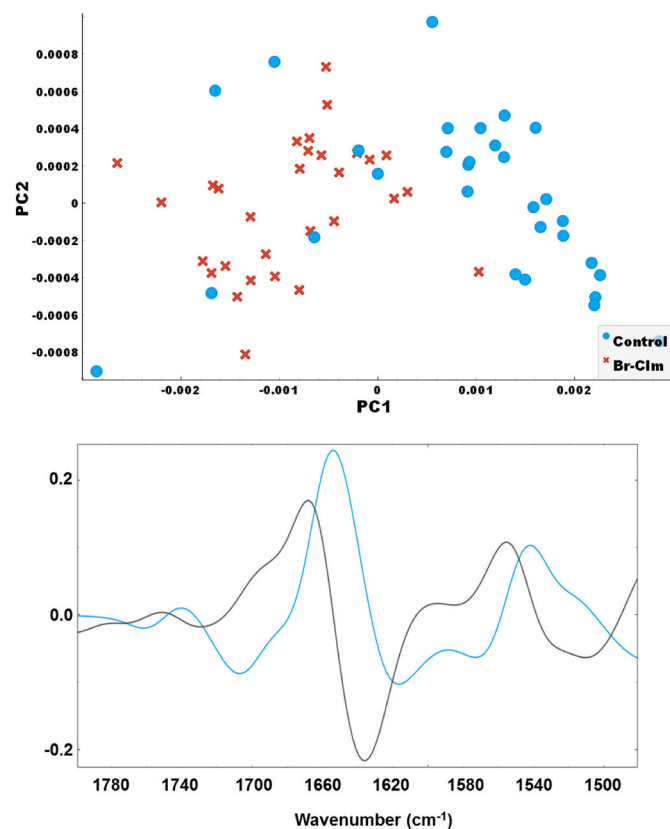


Fig. 5. PCA score plot for the area of 1800–1480  $\text{cm}^{-1}$ , regarding AGS cell lines treated and untreated with Br-Clm (top). Corresponding PCA loadings of the first two components, PC1 (blue) and PC2 (dark gray), regarding the interval of 1800–1480  $\text{cm}^{-1}$  (bottom).

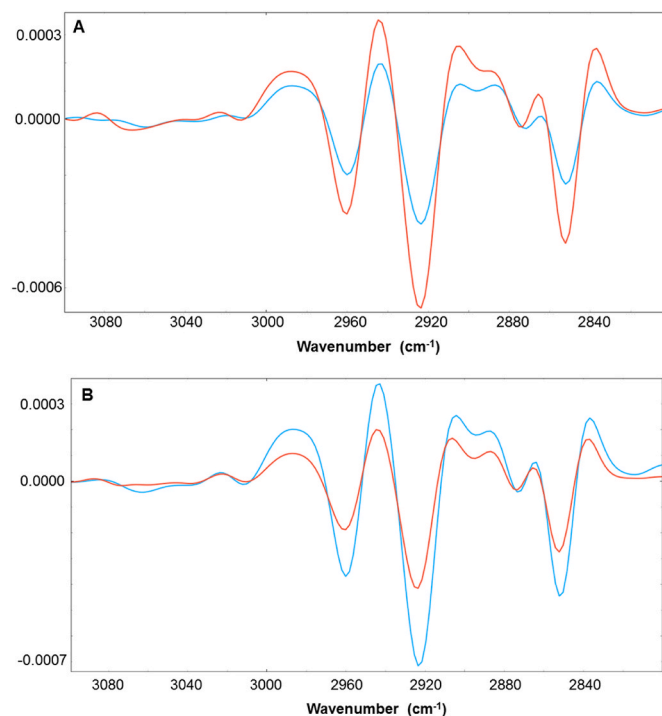


Fig. 6. Second-derivative of the average SR-FTIR spectra, in the area of 3100–2800  $\text{cm}^{-1}$ , of AGS (A) and HaCaT (B) cells, when treated (red) or untreated (blue) with Br-Clm (50  $\mu\text{M}$ ).

where lipids oxidation takes place.

#### 4. Conclusions

Recently, our group have developed a brominated analogue of marine Coelenteramine, which is a metabolic product of the bioluminescent system of marine Coelenterazine. Quite promisingly, we have found that this compound showed relevant anticancer activity toward gastric cancer while having a profile of safety toward noncancer cells. While this compound showed potential for further optimization, we were impaired by the lack of data regarding its actual model of action, which is a hurdle in the development of potential new anticancer drugs.

Given this, we have used here synchrotron radiation-based FTIR to investigate the biochemical changes induced by this Coelenteramine analogue in both cancer and noncancer cells. Synchrotron radiation-based FTIR is a powerful tool that combines the highest spectral and spatial resolution to achieve single-cell resolution. Thus, it can provide detailed information about the composition and conformational organization of different classes of biomolecules.

Herein, we have demonstrated that the brominated Coelenteramine analogue induces significant changes in cellular lipids in gastric cancer cells, which could be attributed to its anticancer mode of action. These changes are related to the increasing extent of oxidative stress and result in changes in membrane polarity, lipid chain packing and lipid composition. Besides, protein conformational changes were observed after treatment, showing more  $\alpha$ -helix structure, as well as the random coils. The same effects were not observed in noncancer cells, which helps to explain the selectivity profile of this molecule. Hence, Br-Clm shows a potential effect in targeting membrane lipids, which could be used to develop anticancer approaches with a profile of safety.

So, synchrotron radiation-based FTIR helped to identify the potential of this analogue in targeting membrane lipids in cancer cells, while proving to be a powerful technique to probe the anticancer mechanism of potential new drugs.

## Declaration of competing interest

The authors declare that they have no known competing financial interests or personal relationships that could have appeared to influence the work reported in this paper.

## Data availability

Data will be made available on request.

## Acknowledgments

The Portuguese “*Fundação para a Ciência e Tecnologia*” (FCT, Lisbon) is acknowledged for funding the project PTDC-QUI/2870/2020, the R&D Unit CIQUP (UIDB/000081/2020 and UIDP/00081/2020), the Associated Laboratory LAQV (UIDB/50006/2020 and UIDP/50006/2020) and the Associated Laboratory IMS (LA/P/0056/2020). L.P.S. and C.M. also acknowledge funding from FCT (CEECINST/00069/2021 and SFRH/BD/143211/2019, respectively). M.A. and T.D. are thankful to the Spanish Ministry of Science and Innovation (MCIN/AEI/10.13039/501100011033) project PID2021-122613OB-I00. ALBA Synchrotron, MIRAS Beamline, is also acknowledged for financial support and good working conditions (AV-2021075222).

## References

- [1] R.L. Siegel, K.D. Miller, N.S. Wagle, A. Jemal, CA: Cancer J. Clin. 73 (2023) 17.
- [2] A. Kreso, J.E. Dick, Cell Stem Cell 14 (2014) 275.
- [3] A. Lin, C.J. Giuliano, A. Palladino, K.M. John, C. Abramowicz, M.L. Yuan, E. L. Sausville, D.A. Lukow, L. Liu, A.R. Chait, Z.C. Galluzzo, C. Tucker, J.M. Sheltzer, Sci. Transl. Med. 11 (2019), eaaw8412.
- [4] M. Muroi, H. Osada, J. Antibiot. 74 (2021) 639.
- [5] C.M. Magalhães, J.C.G. Esteves da Silva, L. Pinto da Silva, ChemPhysChem 17 (2016) 2286.
- [6] M. Vacher, L.F. Galván, B.W. Ding, S. Schramm, R. Berraud-Pache, P. Naumov, N. Ferré, Y.J. Liu, I. Navizet, D. Roca-Sanjuán, W.J. Baader, R. Lindh, Chem. Rev. 118 (2018) 6927.
- [7] A.J. Syed, J.C. Anderson, Chem. Soc. Rev. 50 (2021) 5668.
- [8] M.M. Calabretta, A. Lopreside, L. Montali, M. Zangheri, L. Evangelisti, M. D’Elia, E. Michelini, Anal. Chim. Acta 1200 (2022), 339583.
- [9] P. González-Berdullas, R.B. Pereira, C. Teixeira, J.P. Silva, C.M. Magalhães, J. E. Rodríguez-Borges, D.M. Pereira, J.C.G. Esteves da Silva, L. Pinto da Silva, Int. J. Mol. Sci. 23 (2022) 8271.
- [10] C.M. Magalhães, P. González-Berdullas, M. Pereira, D. Duarte, N. Vale, J.C. G. Esteves da Silva, L. Pinto da Silva, Int. J. Mol. Sci. 23 (2022), 13981.
- [11] L. Pinto da Silva, A. Núñez-Montenegro, C.M. Magalhães, P.J.O. Ferreira, D. Duarte, P. González-Berdullas, J.E. Rodríguez-Borges, N. Vale, J.C.G. Esteves da Silva, Eur. J. Med. Chem. 183 (2019), 111683.
- [12] J. Doherty, G. Cinque, P. Gardner, Appl. Spectrosc. Rev. 52 (2016) 560.
- [13] T. Ducić, C.S. Alves, Z. Vucinić, J.M. Lázaro-Martínez, M. Petković, J. Soto, D. Mutavdzic, M.V.M. Yuso, K. Radotić, M. Algarra, J. Colloid Interface Sci. 626 (2022) 226.
- [14] T. Ducić, M. Ninković, I. Martínez-Rovira, S. Sperling, V. Rohde, D. Dimitrijević, G. V.J. Manas, L. Vaccari, G. Birarda, I. Yousef, Anal. Chem. 94 (2022) 1932.
- [15] M.D. Nesić, T. Ducić, M. Algarra, I. Popović, M. Spetić, M. Gonçalves, M. Petković, Cancers 14 (2022) 1182.
- [16] J. Zhong, W. Yu, Y. Tang, X. Zhou, ACS Omega 7 (2022), 47274.
- [17] I. Yousef, L. Ribó, A. Crisol, I. Sics, G. Ellis, T. Ducic, M. Kreuzer, N. Benseny-Cases, M. Quispe, P. Dumas, S. Lefrançois, T. Moreno, G. García, S. Ferrer, J. Nicolas, M.A. G. Aranda, Synchrotron Radiat. News 30 (2017) 4.
- [18] M.D. Nesić, T. Ducić, M. Gonçalves, M. Spetić, M. Algarra, J. Soto, B. Gemović, T. J. Bandosz, M. Petković, Chem. Biol. Interact. 360 (2022), 109950.
- [19] J. Demsar, T. Turk, A. Erjavec, C. Gorup, T. Hocevar, M. Milutinovic, M. Mozina, M. Polajnar, M. Toplak, A. Staric, et al., J. Mach. Learn. Res. 14 (2013) 2349.
- [20] X. Zhou, J. Zhong, W. Yu, Spectrochim. Acta Mol. Biomol. Spectrosc. 283 (2022), 121773.
- [21] O. Bozkurt, M. Severcan, F. Severcan, Analyst 135 (2010) 3110.
- [22] G. Preta, Front. Cell Dev. Biol. 8 (2020), 571237.
- [23] T. Ducic, S. Stamenkovic, B. Lai, P. Andjus, V. Lucic, Anal. Chem. 91 (2019) 1460.